Epsilon iron oxide: origin of the high coercivity stable low Curie temperature magnetic phase found in heated archeological materials

Lopez-Sanchez, J., McIntosh, G., Osete, M., del Campo, A., Villalain, J., Perez, L., Kovacheva, M. and Rodriguez de la Fuente, O.

J_ID: GGGE Customer A_ID: GGGE21345 Cadmus Art: GGGE21345 Ed. Ref. No.: 2017GC006929 Date: 5-July-17 Stage: Page: 1

AGU PUBLICATIONS

Geochemistry, Geophysics, Geosystems

RESEARCH ARTICLE
10.1002/2017GC006929

Key Points:
- ε-Fe_2O_3, a rare iron oxide polymorph, has been identified in archeological brick and baked clay
- It has been found as part of the γ-Fe_2O-ε-Fe2O3-α-Fe_2O_3 transformation series
- CRS and mineral magnetic measurements have proved a powerful combination for identifying complex magnetic mixtures in natural samples

Supporting Information:
- Supporting Information S1

Correspondence to:
J. López-Sánchez,
jesus.lopez@ucm.es

Citation:
López-Sánchez, J., G. McIntosh, M. L. Osete, A. del Campo, J. J. Villalaín, L. Perez, M. Kovacheva, and O. Rodriguez de la Fuente (2017), Epsilon iron oxide: Origin of the high coercivity stable low Curie temperature magnetic phase found in heated archeological materials, *Geochem. Geophys. Geosyst.*, *18*, doi:10.1002/2017GC006929.

Received 22 MAR 2017
Accepted 19 JUN 2017
Accepted article online 1 JUL 2017

Epsilon iron oxide: Origin of the high coercivity stable low Curie temperature magnetic phase found in heated archeological materials

J. López-Sánchez[1,2], G. McIntosh[3], M. L. Osete[4,5], A. del Campo[6], J. J. Villalaín[7], L. Perez[1,2], M. Kovacheva[8], and O. Rodriguez de la Fuente[1,2,9]

[1]Departamento de Física de Materiales, Universidad Complutense de Madrid, Madrid, Spain, [2]Unidad Asociada IQFR (CSIC)-UCM, Madrid, Spain, [3]School of Human and Life Sciences, Canterbury Christ Church University, Canterbury, UK, [4]Departamento de Física de la Tierra, Astronomía y Astrofísica I (Geofísica y Meteorología), Madrid, Spain, [5]Instituto de Geociencias (UCM-CSIC), Universidad Complutense de Madrid, Madrid, Spain, [6]Instituto de Cerámica y Vidrio, ICV-CSIC, Madrid, Spain, [7]Departamento de Física, Universidad de Burgos, Burgos, Spain, [8]National Institute of Geophysics, Geodesy and Geography, BAS, Sofia, Bulgaria, [9]Instituto de Magnetismo Aplicado, UCM-CSIC-ADIF, Las Rozas, Madrid, Spain

Abstract The identification of epsilon iron oxide (ε-Fe_2O_3) as the low Curie temperature high coercivity stable phase (HCLST) carrying the remanence in heated archaeological samples has been achieved in samples from two archaeological sites that exhibited the clearest evidence of the presence of the HCSLT. This uncommon iron oxide has been detected by Confocal Raman Spectroscopy (CRS) and characterized by rock magnetic measurements. Large numbers of ε-Fe_2O_3 microaggregates (in CO) or isolated clusters (in HEL) could be recognized, distributed over the whole sample, and embedded within the ceramic matrix, along with hematite and pseudobrookite and with minor amounts of anatase, rutile, and maghemite. Curie temperature estimates of around 170°C for CO and 190°C for HEL are lower than for pure, synthetic ε-Fe_2O_3 (227°C). This, together with structural differences between the Raman spectra of the archeologically derived and synthetic samples, is likely due to Ti substitution in the ε-Fe_2O_3 crystal lattice. The γ-Fe_2O_3-ε-Fe_2O_3-α-Fe_2O_3 transformation series has been recognized in heated archeological samples, which may have implications in terms of their thermal history and in the factors that govern the formation of ε-Fe_2O_3.

1. Introduction

Archeomagnetism provides important constraints on the local and global geomagnetic field variation during the historical past, thus contributing to the study of the geodynamo and to archeomagnetic dating. Its physical basis is connected to the magnetic properties of heated archeological materials and to the presence of stable magnetic remanence acquired at the time of the heating process. Detailed knowledge of the magnetic carriers in ceramics, bricks, and baked clays is important as they impact the remanence stability during laboratory treatment, the correct determination of the archeomagnetic signal and the suitability of the material for paleointensity determination. Generally speaking, a mixture of iron oxides, each of which possesses particular magnetic properties, carries the magnetic remanence. The archeomagnetic literature points mainly to magnetically soft (titano) magnetites and maghemite as the main components of the mixtures, with magnetically hard hematite and goethite being of lesser importance [e.g., *Cui et al.*, 1997].

In addition to these well-known magnetic minerals, a widespread occurrence of a novel, high coercivity (>600 mT), thermally stable, low unblocking temperature ($\leq$200–240°C) magnetic phase in well-heated archeological material was reported by *McIntosh et al.* [2007]. This so-called HCSLT phase occurred over a broad geographical and temporal range in both bricks and baked clays [*McIntosh et al.*, 2011]. While the thermal stability distinguishes the HCSLT phase from goethite, an unambiguous identification could not be provided [*McIntosh et al.*, 2007, 2011], with candidates such as hemoilmenite ($Fe_{2-y}Ti_yO_3$) with a Ti content of $y \approx 0.5$, magnetic ferri-cristobalite [*Moskowitz and Hargraves*, 1984], epsilon iron oxide (ε-Fe_2O_3), and cation-substituted hematite being discussed by the authors. In the context of the present study, it is worth pointing out that ε -Fe_2O_3 [*Petersen et al.*, 1987] was the candidate that was least favored by the authors—based mainly on Mössbauer spectroscopy [*McIntosh et al.*, 2011; *Donadini et al.*, 2007]. This was reassessed

ID: vijayalakshmi.s Time: 12:34 I Path: //chenas03.cadmus.com/Home$/vijayalakshmi.s$/JW-GGGE170117

J_ID: GGGE Customer A_ID: GGGE21345 Cadmus Art: GGGE21345 Ed. Ref. No.: 2017GC006929 Date: 5-July-17 Stage: Page: 2

in light of a recent study by *Dejoie et al*. [2014], who identified the presence of ε-Fe_2O_3 in black glazed Jian wares from the Fujian province of China.

ε-Fe_2O_3 is a rare, metastable polymorph of Fe_2O_3 whose magnetic properties (high-coercive field and low Curie temperature) are compatible with the HCSLT phase. It is ferrimagnetic, with a saturation magnetization around 15A m^2 kg^{-1}, mainly existing in a nanometric form [*Ohkoshi et al*., 2005]. It has an orthorhombic structure with lattice parameters $a = 5.095$ Å, $b = 8.789$Å, and $c = 9.437$ Å. The structure has four nonequivalent cation positions, one tetrahedrally and three octahedrally coordinated, all of them with a certain degree of distortion that is believed to be crucial for the magnetic properties and their thermal evolution [*MacHala et al*., 2011].

Although the magnetic behavior of ε-Fe_2O_3 is not fully understood, it is well established that it undergoes two magnetic transitions, one above and one below room temperature. It is ferrimagnetic at room temperature and has a Curie temperature around 227°C. A low temperature magnetic transition between two different magnetically ordered phases has also been reported at around −163°C [*Gich et al*., 2005]. It possesses a large magnetocrystalline anisotropy, which is reflected in a maximum coercive force of around 2 T at room temperature. Transition temperatures and coercive force both strongly depend on particle size [*Ohkoshi et al*., 2015], doping or cation substitution [*Namai et al*., 2012].

Confocal Raman Spectroscopy (CRS) is a nondestructive technique that provides local structural and chemical information with crystallinity, amount of material or phase identification being the most typical analyses [*Jubb and Allen*, 2010]. In addition, it permits the scanning of large in-plane (XY) areas as well as in Z-depth. Surprisingly, it is not a common tool in paleomagnetism and rock magnetism in comparison to other techniques such as X-ray Diffraction (XRD), Mössbauer Spectroscopy or Energy-dispersive X-ray Spectroscopy (EDX). XRD and Mössbauer Spectroscopy have the inconvenience of measuring bulk samples, which might hinder the identification of the less representative components (in sample percentage), as is commonly the case for the magnetic minerals that typically dominate the bulk magnetic properties. EDX gives compositional information of specific elements but does not reveal which polymorph is present or distinguish components with similar element percentages. A major advantage of CRS is that it permits precise microstructural and mineralogical identification, as well as the determination of structural modifications and chemical environments of the different mineralogical phases which may coexist in baked clay materials [*Colomban*, 2003; *Bellot-Gurlet et al*., 2009; *Medeghini et al*., 2013].

With this in mind, the present study describes the results of micro-Raman XY-mappings that have been carried out on samples from two archaeological sites that exhibited the clearest evidence of the presence of the HCSLT phase described in *McIntosh et al*. [2007]. Complementary rock magnetic results from the same samples are also presented, along with supporting information summarizing previous results. The objectives are to conclusively identify the HCSLT phase and to demonstrate the potential of CRS in identifying the components of complex magnetic mixtures in natural samples.

2. Experimental Procedures and Studied Samples

Raman spectra were acquired using a confocal Raman microscope (ALPHA 300RA, WITEC, at the Institute of Ceramics and Glass—Spanish National Research Council (ICV-CSIC)), with a Nd:YAG laser light source (532 nm) in p-polarization. The optical resolution of the system is approximately 200 nm in the lateral direction and 500 nm in the vertical direction. The spectral resolution of the system is 0.02 cm^{-1}. Spectra were acquired in the spectral range of $0 - 3600$ cm^{-1} by using a 600g mm^{-1} grating. Samples were mounted on a piezo-driven scan platform with a positioning accuracy of 4 nm in the lateral direction and 0.5 nm in the vertical direction. Raman measurements were performed at room temperature, working with a 100× objective numerical aperture of 0.95. The laser excitation power chosen was set at 0.7 mW in order to avoid unwanted phase transformations induced by the laser. Data were analyzed using the WITEC Control Plus software.

Thermomagnetic curves were measured in air between room temperature and 700°C using a variable field translation balance (MMVFTB, Magnetic Measurements, at the Burgos palaeomagnetic laboratory, University of Burgos), with applied fields of approximately 1 T. The curves were analyzed using the RockMagAnalyzer software [*Leonhardt*, 2006]. Magnetic hysteresis loops were measured using a SQUID magnetometer

ID: vijayalakshmi.s Time: 12:34 I Path: //chenas03.cadmus.com/Home$/vijayalakshmi.s$/JW-GGGE170117

J_ID: GGGE Customer A_ID: GGGE21345 Cadmus Art: GGGE21345 Ed. Ref. No.: 2017GC006929 Date: 5-July-17 Stage: Page: 3

(MPMS, Quantum Design, at the CAI de Técnicas Físicas, Complutense University of Madrid), with a maximum applied field of 5 T. Magnetic hysteresis loops were measured at −193°C, −133°C and room temperature (see supporting information). The same instrument was used to measure field cooled (FC) and zero field cooled (ZFC) magnetization curves. For the FC curve, a room temperature isothermal remanence was acquired in a 5 T applied field, the sample was cooled to −269°C in a 20 mT applied field, then the variation of the remanence with temperature was measured during warming to room temperature in a 20 mT field. For the ZFC curve, the procedure was the same except that cooling and warming was performed in the absence of an applied field.

Stepwise thermal demagnetization of orthogonal IRMs [*Lowrie*, 1990] up to 700°C was carried out using TSD-1 (Schönstedt) and MMTD-80 (Magnetic Measurements) thermal demagnetizers, a Minispin spinner magnetometer (Molspin Ltd.) and an IM10–30 impulse magnetiser (ASC Scientific), all at the Complutense University of Madrid. After completion of the first demagnetization up to 700°C, the experiment was repeated in order to test the thermal stability of the orthogonal IRM fractions.

Samples from two archeological sites have been studied. CO_62_5 (labeled CO throughout the text) samples come from a baked clay block used in the construction of a medieval kiln from Cordoba (Spain). HEL1 (labeled HEL) samples come from a modern brick (1906 AD, *Donadini et al.* [2007]) from Helsinki (Finland). Both were investigated by *McIntosh et al.* [2007, 2011] and exhibited magnetic properties strongly influenced by the presence of the HCSLT phase. It is important to mention that the selected samples were not isolated examples: evidence for this magnetic phase was documented in at least 16 archaeological features across Europe [*McIntosh et al.*, 2007, 2011], in Brazil [*Hartmann et al.*, 2011], in Western Africa [*Donadini et al.*, 2007; *Mitra et al.*, 2013; *Donadini et al.*, 2015], in Mexico [*Kapper et al.*, 2016], and Eastern China [*Cai et al.*, 2014, 2016]. Therefore, it seems that the presence of this magnetic phase is globally widespread around the world.

3. Results

3.1. Magnetic Properties

Magnetic measurements corroborate the results of *McIntosh et al.* [2007, 2011]: the magnetic mineralogy is a mixture of high and low coercivity phases, the contribution of each varying from sample to sample. Wasp-waisted hysteresis loops at room temperature are observed in samples from both sites (Figures 1g–1h). The high coercivity phase only approaches saturation at applied fields larger than 4–5 T. Wasp-waisting is observed in the hysteresis loops down to −193°C (supporting information Figure S1a), confirming the low and high coercivity contribution even at low temperatures.

The results of the low temperature remanence measurements are given in the supporting information Figure S1b. For the ZFC curve, magnetization increases to maximum values around −173°C without showing any clear transitions, then decreasing with temperature to −253°C and finally increasing. There are no clear transitions in the FC curve. The lack of clear transitions in either curve prevents the identification of the magnetic phases from low temperature experiments.

Thermomagnetic curves show evidence for two magnetic phases, both having a high degree of thermal stability (Figures 1a and 1b). Curie temperature estimates for the lower temperature phase of 169°C for CO and 188°C for HEL are in close agreement with the IRM unblocking temperature of the HCSLT phase (Figure 2). These temperatures are slightly lower than the value of 227°C usually ascribed to ε-Fe_2O_3. Curie temperature estimates for the higher temperature phase are 552°C for CO and 581°C for HEL. They are consistent with the unblocking temperatures of the low coercivity IRM fraction (Figure 2) and close to the values expected for magnetite (Fe_3O_4) or maghemite (γ-Fe_2O_3) with a small amount of cation substitution. One final observation from the IRM demagnetization curves is that the relative fraction of ε-Fe_2O_3 and the low coercivity fraction are highly heterogeneous between CO samples (Figure 2). For example, in sample CO.7A the IRM intensity is dominated by the high coercivity fraction (Figure 2a) being the low coercivity phase of very low intensity (Figure 2b). In contrast, in samples CO16A and CO12A, the low coercivity phase dominates the IRM although the HCSLT phase is also present.

3.2. Confocal Raman spectroscopy

In both samples, the results indicate the presence of extensive areas dominated by quartz, feldspars, and hematite (α-Fe_2O_3). This is also supported by XRD spectra (see supporting information Figure S2). In

ID: vijayalakshmi.s Time: 12:34 I Path: //chenas03.cadmus.com/Home$/vijayalakshmi.s$/JW-GGGE170117

J_ID: GGGE Customer A_ID: GGGE21345 Cadmus Art: GGGE21345 Ed. Ref. No.: 2017GC006929 Date: 5-July-17 Stage: Page: 4

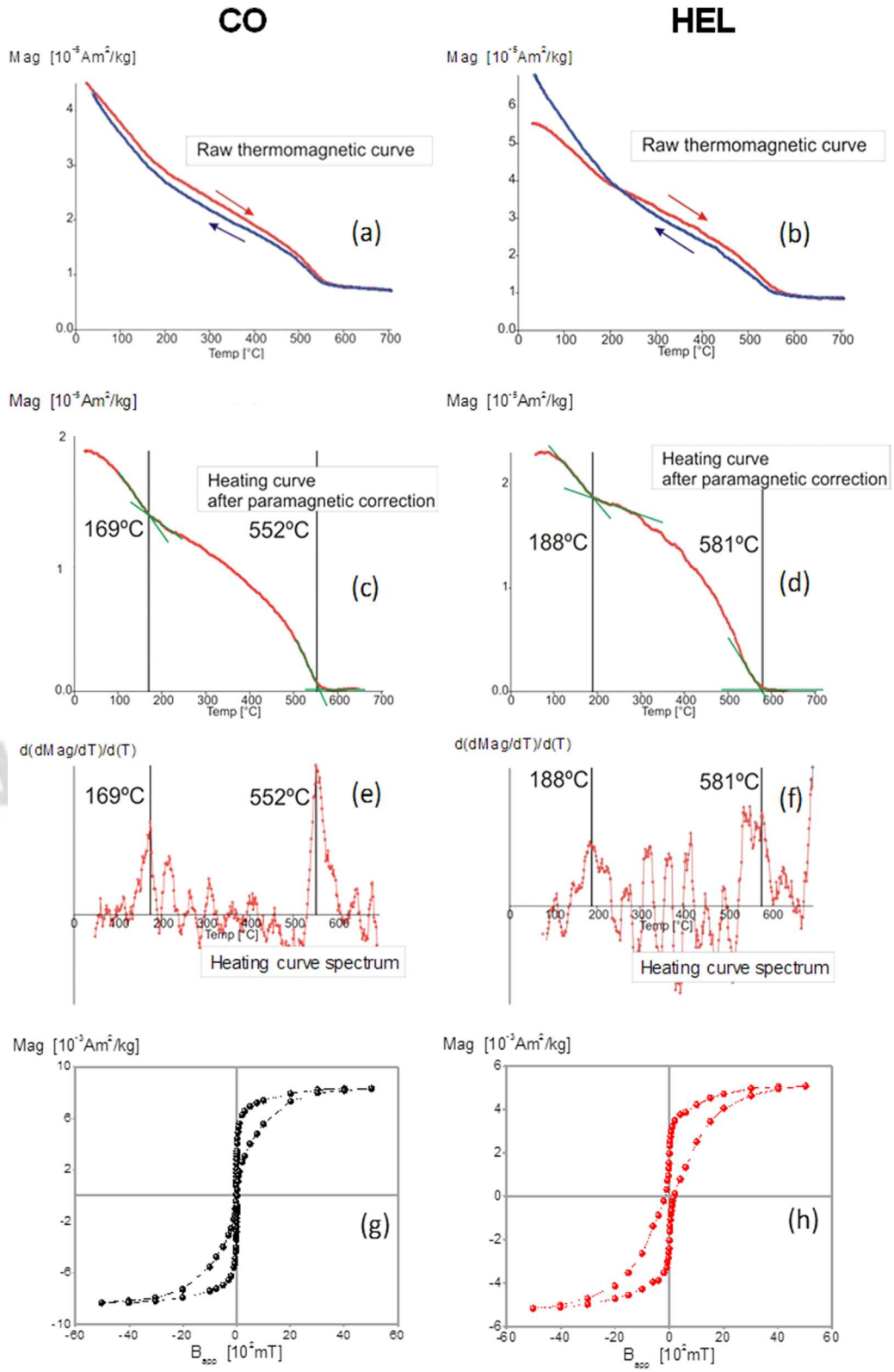

Figure 1. Rock magnetic analyses of representative HEL and CO samples. (a and b) Thermomagnetic curves obtained in a field of 1 T. (c and d) Heating curve corrected for the paramagnetic contribution and Curie temperature determination. (e and f) Second derivative of the heating curve. (g and h) Hysteresis curves at room temperature (corrected by the paramagnetic contribution).

ID: vijayalakshmi.s Time: 12:34 I Path: //chenas03.cadmus.com/Home$/vijayalakshmi.s$/JW-GGGE170117

J_ID: GGGE Customer A_ID: GGGE21345 Cadmus Art: GGGE21345 Ed. Ref. No.: 2017GC006929 Date: 5-July-17 Stage: Page: 5

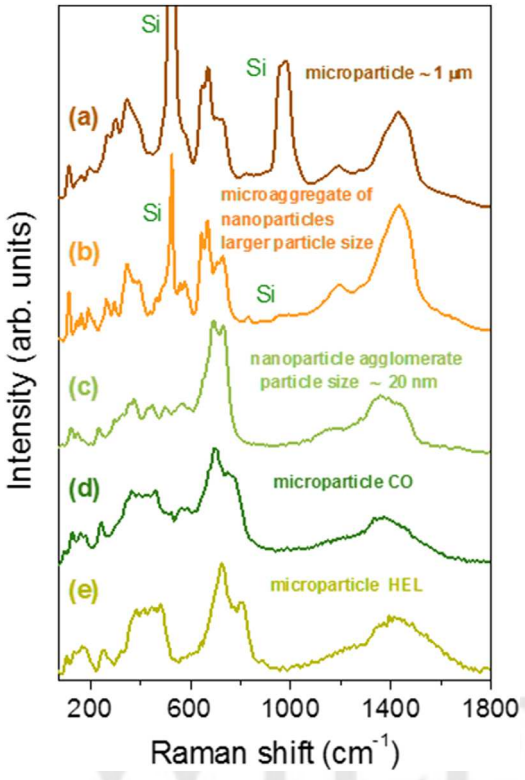

Figure 2. Representative thermal demagnetization of orthogonal isothermal and natural remanences from different CO samples (7A, 12A, and 16A). (top) Stepwise Thermal demagnetization of two orthogonal IRMs in CO samples (a) intensity decay ofthe high coercivity IRM fraction (the 0.3–2 T), showing the HCSLT phase. (b) Intensity decay of the low coercivity magnetic component. (bottom) Thermal Demagnetization of the Natural remanent magnetization of a representative sample from CO: (c) Zijderveld diagram and (d) intensity decay. In Figure 2c, closed and open symbols represent projection in the horizontal and vertical planes, respectively. Initial NRM of sample displayed in Figure 2c is 1.35 A/m.

addition, large numbers of microaggregates (CO) or isolated clusters (HEL) of pseudobrookite (Fe_2TiO_5), hematite, and ε-Fe_2O_3 can be observed by CRS, along with minor amounts of titanium dioxide (anatase and rutile) and maghemite. The occurrence of magnetite, ulvöspinel (Fe_2TiO_4) or ilmenite ($FeTiO_3$) has not been detected in any of the areas investigated by CRS measurements, nor are they observed in the XRD spectra (see supporting information Figure S2).

A representative area of CO is depicted in the optical image in Figure 3a. Scans performed on the yellow square show Raman spectra corresponding to maghemite, ε-Fe_2O_3, pseudobrookite, and hematite microaggregates (Figures 3b and 3c). These minerals can be clearly distinguished and no mixing between them has been detected. F3

HEL samples exhibit relatively large areas of ε-Fe_2O_3 microaggregates and isolated clusters (Figure 4a) that are distributed over the whole sample and enclosed within the ceramic matrix. Micrometric ε-Fe_2O_3 grains completely surrounded by hematite are clearly observed (Figures 4b and 4c). In order to compare the structural properties of these samples with those obtained from other works, a Lorentzian fitting is performed on the average Raman spectrum acquired in CO_62_5 and HEL1. The position of the Raman shift is displayed on top of the peaks for each compound found in the areas selected. Comparing to other works where the Raman spectra are collected from pure PB [5,6,7], hematite [8], epsilon (ε-Fe2O3) [10], it is observed Raman shift deviations being more pronounced for CO_62_5. F4

Lorentzian fitting has been performed on the average Raman spectra of the CO and HEL samples. The position of the Raman shift is displayed on top of the major peaks for each mineral found in the selected areas (Figures 3c and 4c). Comparing to other works where the Raman spectra are collected from pseudobrookite [*Wang et al*., 2016; *Bersani et al*., 2000; *Prinsloo et al*., 2011], hematite [*Leon et al*., 2010a, 2010b], ε-Fe_2O_3 [*Dejoie et al*., 2014; *López-Sánchez et al*., 2016a], and maghemite [*Bellot-Gurlet et al*., 2009], Raman shift deviations generally toward higher wave numbers are observed for both CO and HEL. Wavelength deviations were larger for CO than for HEL especially for ε-Fe_2O_3 (Figure 5). The shift of the bands could be related to stress induced by the encasing ceramic matrix [*Colomban and Havel*, 2002; *Rubio*, 2015]. In addition, the number of the Raman bands is different than expected for pure phases, indicating that the crystal lattice has different vibration frequencies. This could be explained in terms of cation substitution, which leads to alteration of the lattice vibration frequencies and is reflected in band shifts and/or the emergence of new bands in the Raman spectrum. AQ2 F5

4. Discussion

The CRS results clearly show the presence of ε-Fe_2O_3 in the CO and HEL samples and so confirm the identity of the HCSLT phase described by *McIntosh et al*. [2007, 2011]. Relatively large areas of ε-Fe_2O_3 microaggregates (Figure 3b) and isolated clusters (Figure 4b) are distributed throughout both samples, embedded within the ceramic matrix. It is noticeable that the ε-Fe_2O_3 Raman spectra are analogous with those

ID: vijayalakshmi.s Time: 12:34 I Path: //chenas03.cadmus.com/Home$/vijayalakshmi.s$/JW-GGGE170117

J_ID: GGGE Customer A_ID: GGGE21345 Cadmus Art: GGGE21345 Ed. Ref. No.: 2017GC006929 Date: 5-July-17 Stage: Page: 6

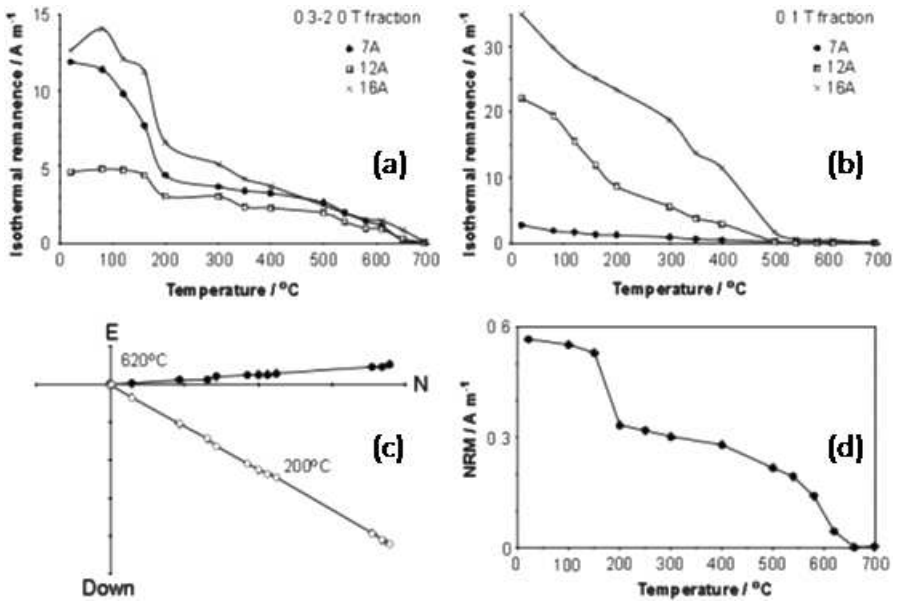

Figure 3. (a) Optical image from sample CO. (b) In-plane Raman intensity image obtained from mapping the region marked with a yellow square in Figure 3a, measuring different single Raman spectra taken each 100 nm with an integration time of 3 s. Maghemite (blue), ε-Fe_2O_3(green), pseudobrookite (violet) and hematite (red) were all detected. (c) Average Raman spectra obtained from in-plane Raman image. Positions of the Raman shifts have been calculated by Lorentzian fitting in each case and the main peaks are labeled.

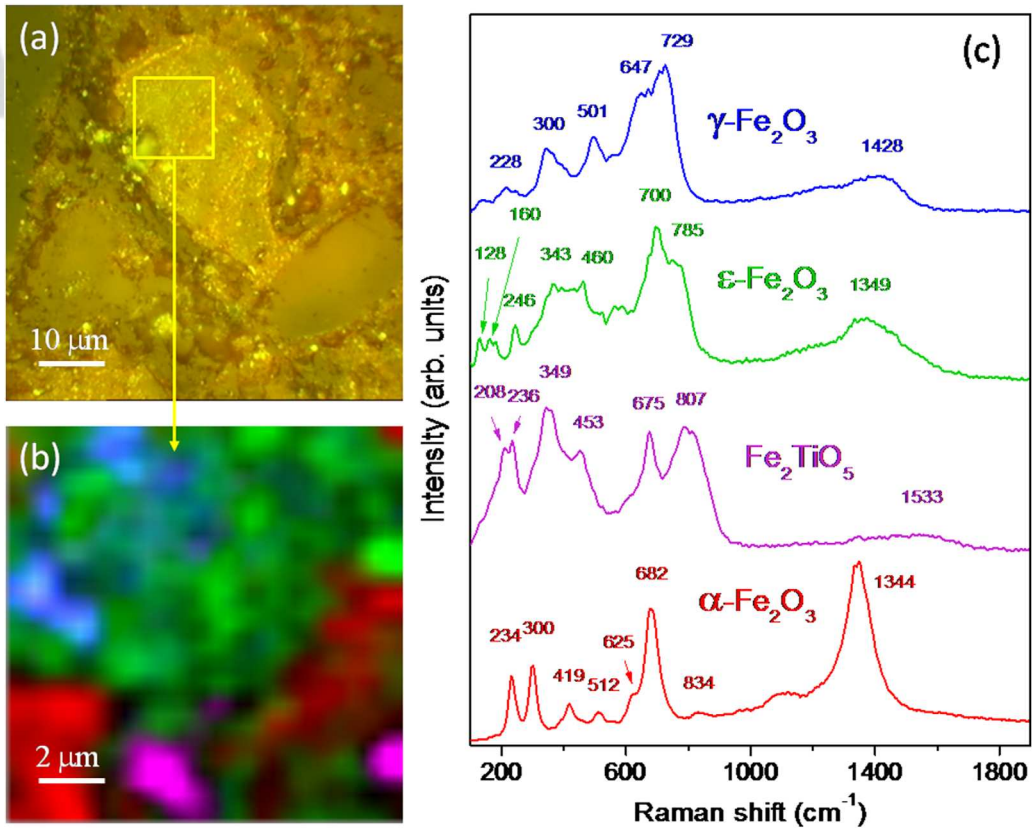

Figure 4. (a) Optical image of sample HEL. (b) In-plane Raman intensity image obtained from mapping the region marked with a yellow square in Figure 4a. (c) Average Raman spectra obtained from in-plane Raman image. See Figure 3 caption for spectra measurement and calculation details.

ID: vijayalakshmi.s Time: 12:35 I Path: //chenas03.cadmus.com/Home$/vijayalakshmi.s$/JW-GGGE170117

J_ID: GGGE Customer A_ID: GGGE21345 Cadmus Art: GGGE21345 Ed. Ref. No.: 2017GC006929 Date: 5-July-17 Stage: Page: 7

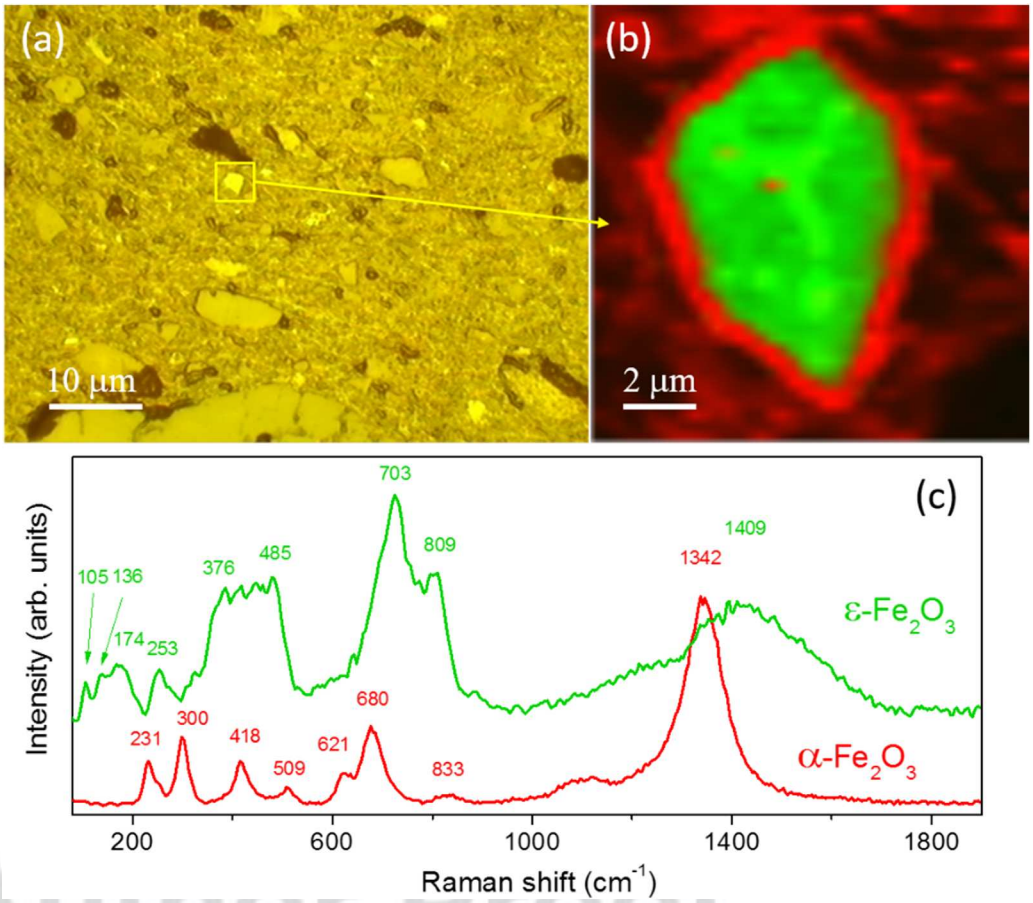

Figure 5. Raman spectra from synthetic ε-Fe_2O_3. Comparison between different Raman spectra collected from different samples which contain ε-Fe_2O_3: (a) single microparticle [*López-Sánchez et al*., 2016a], (b) microaggregate of nanoparticles [*López-Sánchez et al*., 2016a], (c) nanoparticle agglomerate [*López-Sánchez et al*., 2016b], (d) microparticle collected from CO (Figure 3c), and (e) microparticle acquired from HEL1 (Figure 4c).

acquired from ancient black-glazed Jian wares, with similar micrometric grain sizes [*Dejoie et al*., 2014]. This highlights the fact that ε-Fe_2O_3 can be formed in archeological baked clays and bricks and is not restricted to particular ceramic types.

When iron(III) oxide particles are grown following a synthetic sol-gel route in a ceramic supporting medium, different polymorphs are formed depending on the degree of agglomeration, the particle size, particle morphology, the presence of coating layers on the particle surface, the presence of dopants and the synthesis temperature [*MacHala et al*., 2011]. Commonly, maghemite nanoparticles are observed as a precursor to ε-Fe_2O_3, which can be considered as an intermediate state prior to hematite formation. When embedded in a silica matrix, the typical temperature ranges over which these polymorphs form are: γ-Fe_2O_3 (below 950°C)-β-Fe_2O_3 (950–1300°C)-α-Fe_2O_3 (above 1300°C) [*Ohkoshi et al*., 2015; *MacHala et al*., 2011]. However, as mentioned, these temperatures depend mostly on the degree of agglomeration, the particle size, and the dopants.

The univectorial nature of the thermal demagnetization curves of the natural remanence of CO samples (Figure 2) indicates that the baked clay must have reached at least 650°C and firing temperatures typically reached in archeological kilns can reach up to 1200°C [e.g., *Tite*, 1969]. This would be sufficient to form ε-Fe_2O_3, based on the transformation temperatures set out above. However, it should be pointed out that these temperatures were obtained for synthetic samples and the ε-Fe_2O_3 transition temperature may well be different in archeological materials.

The Raman band positions obtained in the CO and HEL spectra have been compared to those of an isolated sol-gel synthetic, single phase ε-Fe_2O_3 microparticle (Figure 5) [*Lopez-Sanchez et al*., 2016a]. They are mostly

ID: vijayalakshmi.s Time: 12:35 I Path: //chenas03.cadmus.com/Home$/vijayalakshmi.s$/JW-GGGE170117

J_ID: GGGE Customer A_ID: GGGE21345 Cadmus Art: GGGE21345 Ed. Ref. No.: 2017GC006929 Date: 5-July-17 Stage: Page: 8

shifted toward higher wave numbers, excluding the overtone mode that is at lower wave numbers. The increase of the vibrational frequency means a decrease of the lattice parameter which would then lead to compressive strain [*Rubio*, 2015]. The origin of this Raman shift could be related to the encasing ceramic matrix effect. In addition, the number of the Raman bands is slightly different, which can be explained in terms of cation substitution.

The hematite spectra provide a clue to the identity of the cation substituted into the ε-Fe_2O_3 structure. For hematite, a redshift and broadening of the all Raman modes can also be observed. The intensity of the band located at ~680 cm^{-1} is markedly higher than in other studies (see supporting information Figure S3a) [*Jubb and Allen*, 2010; *Lopez-Sanchez et al*., 2016a]. This can be attributed to the disorder produced by lowering of symmetry [*Rubio*, 2015]. Raman investigations carried out on *terra sigillata* [*Wang et al*., 2016; *Leon et al*., 2010a, 2010b] showed that for the most famous fine ware of the Roman period, the intense E_u(LO) mode and the redshift of the Raman spectra was found to be caused by Ti substitution in the hematite structure. The relative high polarizability of the Ti-O bonds explains the strong activation of the E_u(LO) mode located at ~680 cm^{-1}, even with relatively low Ti content [*Leon et al*., 2010a]. The similarities between the *terra sigillata* and HEL and CO hematite spectra suggest that Ti could also substituted into the hematite found in HEL and CO.

When comparing the HEL and CO hematite spectra to ilmenite ($FeTiO_3$) [*Rull*, 2007] and to synthetic, intermediate compound of the hematite-ilmenite ($(1-x)Fe_2O_3$-$xFeTiO_3$) solid solution series with $x = 0.44$ [*Dennenwaldt et al*., 2015], their spectra are distinct and the number of Raman bands and their positions are different. In contrast, they are similar to typical hematite Raman spectra [*Bellot-Gurlet et al*., 2009], with the exception of the prominent E_u(LO) mode (Figures 3c and 4c) which has been attributed to Ti-O bonds. Therefore, it is suggested that Ti substitution in the HEL and CO samples is present at relatively low ($x < 0.44$) values.

As previously mentioned, ε-Fe_2O_3 is a metastable phase and it is considered as a precursor thermodynamic stage of hematite in the γ-Fe_2O_3-ε-Fe_2O_3-α-Fe_2O_3 series [*MacHala et al*., 2011], at least in synthetic materials. Hence, ε-Fe_2O_3 would be expected to convert into hematite at high temperatures. If the hematite formed in this sequence has low levels of Ti substitution, then it seems reasonable to assume that the precursor ε-Fe_2O_3 had similar levels of substitution. This might then explain the differences found between the ε-Fe_2O_3 and hematite Raman spectra of *Lopez-Sanchez et al*. [2016a] and the present study (Figures 3c and 4c). This would also explain the lower Curie temperatures observed for ε-Fe_2O_3 in HEL (188°C) and CO (169°C) compared to pure samples (227°C, *Lopez-Sanchez et al*. [2016b] and *Cornell and Schwertmann* [1996]).

The relative intensity of the disorder hematite mode for CO is larger than HEL. This effect might be interpreted as a higher Ti content in the hematite structure in CO. This effect in ε-Fe_2O_3 would not only tend to shift all modes towards high wave numbers, but may also induce new vibrational modes because of the structural modification and/or cation substitution. The band located at 246 cm^{-1} in HEL and 253 cm^{-1} in CO would appear to be an example of this, when compared to the pure ε-Fe_2O_3 Raman bands of *López-Sánchez et al*. [2016a]. The lower Curie temperature of ε-Fe_2O_3 in CO compared to that observed in HEL is also consistent with a higher Ti content in CO.

Maghemite has been observed by CRS in CO (Figures 3b and 3c) and would explain the low coercivity phase observed in its hysteresis curve. The second, higher Curie temperature of 552°C seen in the CO thermomagnetic curve (Figures 1b and 1d) is lower than expected for pure maghemite, which is usually found to be around 645°C [*Özdemir and Banerjee*, 1984]. However, it is likely that Curie temperatures are reduced by the influence of impurity interactions or cation substitution [*Dunlop and Özdemir*, 1997; *da Costa et al*., 1995]. In fact, the Raman bands and their positions differ from pure synthetic maghemite microparticles observed in other studies [*Rubio*, 2015] (supporting information Figure S3b). Therefore, if the maghemite had similar Ti substitution as the subsequent ε-Fe_2O_3 and hematite phases then lower Curie temperatures would be expected, as is the case. This would tie the maghemite to the ε-Fe_2O_3 and hematite via the transformation series, with Ti being incorporated into the iron oxides as the transformation initiated.

Maghemite was not found by CRS in HEL (Figures 4b and 4c), although a low coercivity contribution could be seen in its hysteresis curve, along with a Curie temperature of 581°C (Figures 1a and 1c). This may be explained in several different ways. First, maghemite is present elsewhere in the sample and was not present in the areas scanned by CRS due to its heterogeneous distribution. If this is the case, then the Curie

ID: vijayalakshmi.s Time: 12:35 I Path: //chenas03.cadmus.com/Home$/vijayalakshmi.s$/JW-GGGE170117

J_ID: GGGE Customer A_ID: GGGE21345 Cadmus Art: GGGE21345 Ed. Ref. No.: 2017GC006929 Date: 5-July-17 Stage: Page: 9

temperature of 581°C indicates some Ti substitution in the maghemite structure, at levels lower than observed in CO. This would be consistent with the lower Ti content in the ε-Fe_2O_3 in HEL compared to CO, as inferred from its higher Curie temperature. Further support for this is provided by the XRD spectrum obtained from a sister sample from the same HEL brick (named HEL1 in Figure 4b, *McIntosh et al*. [2007]), in which both hematite and maghemite were identified.

Alternatively, maghemite is absent from the sample and the low coercivity phase is magnetite, which has a Curie temperature of 585°C. The magnetite was not observed in the areas scanned during CRS, again due to its heterogeneity. In this scenario, the magnetite is not necessarily associated with the ε-Fe_2O_3-α-Fe_2O_3 series and so does not have similar levels of Ti substitution. The absence of any evidence for magnetite in the HEL XRD spectrum is not necessarily conclusive, as it may be absent due to a heterogeneous distribution or be present in such low concentrations that its XRD signal is too weak to be detected.

Choosing between these two options is not possible based on the data currently available. However, a lack of maghemite in HEL could have interesting consequences concerning its thermal history. By analogy with synthetic samples, it may reflect a higher firing temperature of the HEL brick compared to the CO baked clay. Following *Ohkoshi et al*. [2015] and *MacHala et al*. [2011], maghemite transforms to ε-Fe_2O_3 around 950°C in synthetic samples, so its absence in HEL may indicate firing temperatures sufficiently in excess of 950°C that it has completely transformed. In contrast, it is still present in the CO baked clay because it has been subjected to slightly lower temperatures.

It is important to note that hematite was the most abundant magnetic iron oxide in the studied samples. This would explain why in the Mossbauer spectra of samples containing the HCSLT phase only hematite could be recognized [*McIntosh et al*., 2007; *Donadini et al*., 2007]. Both Mossbauer spectroscopy and XRD are bulk analytical techniques and neither ε-Fe_2O_3 nor maghemite and/or magnetite, the minerals that dominate the magnetic signal in all of the samples, could be conclusively identified in all cases. This, coupled with the possible heterogeneity in the distribution of the strongly magnetic phases, means that it is very difficult to get a complete picture of the magnetic mineralogy. Without this complete picture the thermal evolution of the iron oxides in the samples would be much less clear.

In the present study, the combination of rock magnetic measurements and CRS has proved to be a powerful way of identifying the mixed iron oxides in the samples. The rock magnetic measurements are especially sensitive to the phases with high magnetizations, which is of importance in identifying the carriers of the NRM. CRS can detect all mineral phases and has been of particular use in identifying the complex mixture of oxides present in the studied samples. As such, the present study acts as an example of how CRS can be used to enhance mineral magnetic and therefore archeomagnetic and paleomagnetic studies.

The identification of ε-Fe_2O_3 in both types of archeological material is striking, as isthe observation of the γ-Fe_2O_3-ε-Fe_2O_3-α-Fe_2O_3 transformation series. For synthetic samples, the stability of these polymorphs is particle size dependent, with maghemite being more stable for smaller particles, ε-Fe_2O_3 for intermediate particles and hematite for larger particles [*MacHala et al*., 2011]. Additionally, the thermal evolution of sol-gel synthesis ε-Fe_2O_3 generally leads to the formation of nanometric particles [*López-Sánchez et al*., 2016b]. In contrast, the ε-Fe_2O_3 particles observed in HEL and CO tend to be micrometric (Figures 3b and 4b). One possibility is cation substitution leads to an increase in the stability of ε-Fe_2O_3 and promotes larger particle sizes. This is worthy of further study, as is the γ-ε-α oxide transition temperatures and the parameters that control them. Not only would this help in unravelling the thermal history of archeological material, but also in understanding the synthesis of ε-Fe_2O_3, an industrially attractive substance.

5. Conclusions

1. ε-Fe_2O_3has been found in archeological baked clay (CO) and brick (HEL) samples using CRS and identified as the HCSLT phase observed in many archeological sites around Europe [*McIntosh et al*., 2007, 2011]. The Raman spectra are analogous with those acquired from ancient black-glazed wares [*Dejoie et al*., 2014]
2. The widespread occurrence of hematite has been found in both samples, but due to its lower saturation magnetization it does not make a major contribution to the bulk magnetic properties. These are

ID: vijayalakshmi.s Time: 12:35 I Path: //chenas03.cadmus.com/Home$/vijayalakshmi.s$/JW-GGGE170117

J_ID: GGGE Customer A_ID: GGGE21345 Cadmus Art: GGGE21345 Ed. Ref. No.: 2017GC006929 Date: 5-July-17 Stage: Page: 10

dominated by the presence of ε-Fe_2O_3 and maghemite in the baked clay (CO) and ε-$Fe_2O_3$and either maghemite or magnetite in the brick (HEL).

3. The Raman spectra for both ε-Fe_2O_3 and hematite differ from their pure analogues, which can be attributed to stress induced by the ceramic matrix, impurity interaction and/or cation substitution (probably Ti). The lower Curie temperatures observed in mineral magnetic experiments would seem to confirm the presence of cation substitution in ε-Fe_2O_3 in both samples (CO and HEL) and in maghemite in the baked clay (CO).
4. The use of CRS has permitted the identification of different Fe oxides in both types of sample. Coupled with routine mineral magnetic measurements, this has led to a more complete picture of the magnetic mineralogy and thermal history of the samples.

Acknowledgments

This work has been supported by the MICINN through projects MAT2012–38045-C04–03, MAT2013–48009-C04–01, and CGL2014–54112-R. J. L.S. thanks the FPI fellowship for predoctoral fellowship. Constructive comments and suggestions from anonymous reviewers have highly improved the manuscript and are therefore gratefully acknowledged. Readers can find in the supporting information the low temperature magnetic behavior and the X-ray diffraction pattern corresponding to the HEL sample. A Raman spectra comparison of maghemite and hematite microparticles obtained from these specific samples, with pure maghemite and hematite microparticles coming from synthetic samples is also provided. Raman and rockmag data from HEL and CO samples used in this paper are available from the Web site: http://earthref.org/ERDA/2214/ as well as Raman data from synthetic epsilon, maghemite, and hematite.

References

Bellot-Gurlet, L., D. Neff, S. Réguer, J. Monnier, M. Saheb, and P. Dillmann (2009), Raman studies of corrosion layers formed on archaeological irons in various media, *J. Nano Res.*, *8*, 147–156, doi:10.4028/www.scientific.net/JNanoR.8.147.

Bersani, D., P. P. Lottici, and A. Montenero (2000), A micro-Raman study of iron-titanium oxides obtained by sol-gel synthesis, *J. Mater. Sci.*, *35*(17), 4301–4305, doi:10.1023/A:1004884302755.

Cai, S., L. Tauxe, C. Deng, Y. Pan, G. Jin, J. Zheng, F. Xie, H. Qin, and R. Zhu (2014), Geomagnetic intensity variations for the past 8 kyr: New archaeointensity results from Eastern China, *Earth Planet. Sci. Lett.*, *392*, 217–229, doi:10.1016/j.epsl.2014.02.030.

Cai, S., L. Tauxe, C. Deng, H. Qin, Y. Pan, G. Jin, X. Chen, W. Chen, F. Xie, and R. Zhu (2016), New archaeomagnetic direction results from China and their constraints on palaeosecular variation of the geomagnetic field in Eastern Asia, *Geophys. J. Int.*, *207*(2), 1332–1342, doi:10.1093/gji/ggw351.

Colomban, P. (2003), Lapis lazuli as unexpected blue pigment in Iranian Lâjvardina ceramics, *J. Raman Spectrosc.*, *34*(6), 420–423, doi:10.1002/jrs.1014.

Colomban, P., and M. Havel (2002), Raman imaging of stress-induced phase transformation in transparent ZnSe ceramic and sapphire single crystals, *J. Raman Spectrosc.*, *33*(10), 789–795, doi:10.1002/jrs.919.

Cornell, R. M., and U. Schwertmann (1996), *The Iron Oxides*, 1st ed., Wiley-VHC, Weinhem, Germany.

Cui, Y., K. L. Verosub, A. P. Roberts, and M. Kovacheva (1997), Mineral magnetic studies of archaelogical samples: Implications for sample selection for paleointensity determinations, *J. Geomagn. Geolelectr.*, *49*, 567–585.

da Costa, G. M., E. De Grave, L. H. Bowen, P. M. A. de Bakker, and R. E. Vandenberghe (1995), Temperature dependence of the hyperfine parameters of maghemite and Al-substituted maghemites, *Phys. Chem. Miner.*, *22*(3), 178–185, doi:10.1007/BF00202298.

Dejoie, C., P. Sciau, W. Li, L. Noé, A. Mehta, K. Chen, H. Luo, M. Kunz, N. Tamura, and Z. Liu (2014), Learning from the past: Rare ε-Fe_2O_3 in the ancient black-glazed Jian (Tenmoku) wares, *Sci. Rep.*, *4*, 4941, doi:10.1038/srep04941.

Dennenwaldt, T., et al. (2015), Insights into the structural, electronic, and magnetic properties of $Fe_{2-x}Ti_xO_3/Fe_2O_3$ thin films with x=0.44 grown on Al_2O_3 (0001), *J. Mater. Sci.*, *50*(1), 122–137, doi:10.1007/s10853-014-8572-x.

Donadini, F., M. Kovacheva, M. Kostadinova, L. Casas, and L. J. Pesonen (2007), New archaeointensity results from Scandinavia and Bulgaria. Rock-magnetic studies inference and geophysical application, *Phys. Earth Planet. Inter.*, *165*(3–4), 229–247, doi:10.1016/j.pepi.2007.10.002.

Donadini, F., V. Serneels, L. Kapper, and A. El Kateb (2015), Directional changes of the geomagnetic field in West Africa: Insights from the metallurgical site of Korsimoro, *Earth Planet. Sci. Lett.*, *430*, 349–355, doi:10.1016/j.epsl.2015.08.030.

Dunlop, D. J., and Ö. Özdemir (1997), Rock Magnetism: Fundamentals and Frontiers, Intergov. Panel on Clim. Change, Cambridge Univ. Press, Cambridge, U. K.

Gich, M., A. Roig, C. Frontera, E. Molins, J. Sort, M. Popovici, G. Chouteau, D. Martín y Marero, and J. Nogués (2005), Large coercivity and low-temperature magnetic reorientation in ε-Fe_2O_3 nanoparticles, *J. Appl. Phys.*, *98*, 1–5, doi:10.1063/1.1997297.

Hartmann, G. A., A. Genevey, Y. Gallet, R. I. F. Trindade, M. Le Goff, R. Najjar, C. Etchevarne, and M. C. Afonso (2011), New historical archeointensity data from Brazil: Evidence for a large regional non-dipole field contribution over the past few centuries, *Earth Planet. Sci. Lett.*, *306*(1–2), 66–76, doi:10.1016/j.epsl.2011.03.030.

Jubb, A. M., and H. C. Allen (2010), Vibrational spectroscopic characterization of hematite, maghemite, and magnetite thin films produced by vapor deposition, *ACS Appl. Mater. Interfaces*, *2*(10), 2804–2812, doi:10.1021/am1004943.

Kapper, K. L., V. Serneels, F. Donadini, E. Tema, A. Goguitchaichvili, and J. Morales (2016), Archeointensity and archeodirectional determinations from ancient iron kilns located in west africa, *Latinmag Lett.*, *6*, 1–8.

Leon, Y., C. Lofrumento, A. Zoppi, R. Carles, E. M. Castellucci, and P. Sciau (2010a), Micro-Raman investigation of terra sigillata slips: A comparative study of central Italian and southern Gaul productions, *J. Raman Spectrosc.*, *41*(11), 1550–1555, doi:10.1002/jrs.2678.

Leon, Y., P. Sciau, P. Goudeau, N. Tamura, S. Webb, and A. Mehta (2010b), The nature of marbled Terra Sigillata slips: A combined μXRF and μXRD investigation, *Appl. Phys. A*, *99*(2), 419–425, doi:10.1007/s00339-010-5628-x.

Leonhardt, R. (2006), Analyzing rock magnetic measurements: The RockMagAnalyzer 1.0 software, *Comput. Geosci.*, *32*(9), 1420–1431, doi:10.1016/j.cageo.2006.01.006.

López-Sánchez, J., A. Muñoz-Noval, A. Serrano, M. Abuín, J. de la Figuera, J. F. Marco, L. Pérez, N. Carmona, and O. Rodríguez de la Fuente (2016a), Growth, structure and magnetism of e-Fe_2O_3 in nanoparticle form, *RSC Adv.*, *6*, 46380, doi:10.1039/c6ra01912a.

López-Sánchez, J., A. Serrano, A. del Campo, M. Abuín, O. Rodríguez de la Fuente, and N. Carmona (2016b), Sol-gel synthesis and micro-Raman characterization of ε-Fe_2O_3 micro- and nanoparticles, *Chem. Mater.*, *28*, 511–518, doi:10.1021/acs.chemmater.5b03566.

MacHala, L., J. Tuček, and R. Zbořil (2011), Polymorphous transformations of nanometric iron(III) oxide: A review, *Chem. Mater.*, *23*(14), 3255–3272, doi:10.1021/cm200397g.

McIntosh, G., M. Kovacheva, G. Catanzariti, M. L. Osete, and L. Casas (2007), Widespread occurrence of a novel high coercivity, thermally stable, low unblocking temperature magnetic phase in heated archeological material, *Geophys. Res. Lett.*, *34*, L21302, doi:10.1029/2007GL031168.

McIntosh, G., M. Kovacheva, G. Catanzariti, F. Donadini, and M. L. Osete (2011), High coercivity remanence in baked clay materials used in archeomagnetism, *Geochem. Geophys. Geosyst.*, *12*, Q02003, doi:10.1029/2010GC003310.

ID: vijayalakshmi.s Time: 12:35 I Path: //chenas03.cadmus.com/Home$/vijayalakshmi.s$/JW-GGGE170117

Medeghini, L., S. Mignardi, C. De Vito, D. Bersani, P. P. Lottici, M. Turetta, J. Costantini, E. Bacchini, M. Sala, and L. Nigro (2013), The key role of micro-Raman spectroscopy in the study of ancient pottery: The case of pre-classical Jordanian ceramics from the archaeological site of Khirbet al-Batrawy, *Eur. J. Mineral.*, *25*(5), 881–893, doi:10.1127/0935-1221/2013/0025-2332.

Mitra, R., L. Tauxe, and S. Keech McIntosh (2013), Two thousand years of archeointensity from West Africa, *Earth Planet. Sci. Lett.*, *364*, 123–133, doi:10.1016/j.epsl.2012.12.027.

Moskowitz, B. M., and R. B. Hargraves (1984), Magnetic cristobalite (?): A possible new magnetic phase produced by the thermal decomposition of nontronite, *Science*, *225*, 1152–1154.

Namai, A., et al. (2012), Hard magnetic ferrite with a gigantic coercivity and high frequency millimetre wave rotation, *Nat. Commun.*, *3*, 1035, doi:10.1038/ncomms2038.

Ohkoshi, S. I., S. Sakurai, J. Jin, and K. Hashimoto (2005), The addition effects of alkaline earth ions in the chemical synthesis of ε-Fe_2O_3 nanocrystals that exhibit a huge coercive field, *J. Appl. Phys.*, *97*(10), 8–11, doi:10.1063/1.1855615.

Ohkoshi, S. I., et al. (2015), Nanometer-size hard magnetic ferrite exhibiting high optical-transparency and nonlinear optical-magnetoelectric effect, *Sci. Rep.*, *5*, 14414.

Özdemir, O., and S. K. Banerjee (1984), High temperature stability of maghemite (g-Fe_2O_3) reflections inversion, *Geophys. Res. Lett.*, *11*(3), 161–164, doi:10.1029/GL011i003p00161.

Petersen, N., N. Schembera, E. Schmidbauer, and H. Vali (1987). Magnetization, Mössbauer spectroscopy and structural studies of a ferrimagnetic Fe-oxide formed by heating nontronite in air, *Phys. Chem. Miner.*, *14*, 118–121.

Prinsloo, L. C., P. Colomban, J. D. Brink, and I. Meiklejohn (2011), A Raman spectroscopic study of the igneous rocks on Marion island: A possible terrestrial analogue for the geology on Mars, *J. Raman Spectrosc.*, *42*(4), 626–632, doi:10.1002/jrs.2756.

Rubio, A. S. (2015), *Modified Au-Based Nanomaterials Studied by Surface Plasmon Resonance Spectroscopy*, *Springer Theses*, Springer Int. Publ., Switzerland, doi:10.1007/978-3-319-19402-8.

Rull, F., J. Martinez-Frias, and J. A. Rodriguez-Losada (2007), Micro-Raman spectroscopic study of El Gasco pumice, western Spain, *J. Raman Spectrosc.*, *38*, 239–244, doi:10.1002/jrs.1628.

Wang, T., C. Sanchez, J. Groenen, and P. Sciau (2016), Raman spectroscopy analysis of terra sigillata: The yellow pigment of marbled sigillata, *J. Raman Spectrosc.*, *47*, 1522–1527, doi:10.1002/jrs.4906.

AQ1: Please note that the references Lowrie [1990] and Tite [1969] are not listed in the reference list. Kindly list the references or delete the reference citations.

AQ2: Please note that the reference Leon et al. [2010] has been changed to Leon et al. [2010a, 2010b] as per the reference list. Kindly check whether is OK as done.

AQ3: Please confirm that given names (red) and surnames/family names (green) have been identified correctly.

AQ4: Author: Please complete the Publication Fee Consent Form included with your article and return to the Production Editor with your proofs. Please use any version of Adobe Acrobat Pro or Reader 11 or higher to edit the form. Reader can be downloaded free at: http://www.adobe.com/products/acrobat/readstep2.html.

AQ5: AUTHOR: Please verify that the linked ORCID identifiers are correct for each author. The ORCID ID for 'Villalaín' seems to be invalid. Please check and supply the correct ORCID ID.

Funding Info Query Form

Please confirm that the funding sponsor list below was correctly extracted from your article: that it includes all funders and that the text has been matched to the correct FundRef Registry organization names. If a name was not found in the FundRef registry, it may be not the canonical name form or it may be a program name rather than an organization name, or it may be an organization not yet included in FundRef Registry. If you know of another name form or a parent organization name for a "not found" item on this list below, please share that information.

FundRef name	FundRef Organization Name
MICINN	Ministerio de Ciencia e Innovación

WILEY

USING e-ANNOTATION TOOLS FOR ELECTRONIC PROOF CORRECTION

Required software to e-Annotate PDFs: Adobe Acrobat Professional or Adobe Reader (version 8.0 or above). (Note that this document uses screenshots from Adobe Reader DC.)
The latest version of Acrobat Reader can be downloaded for free at: http://get.adobe.com/reader/

Once you have Acrobat Reader open on your computer, click on the Comment tab (right-hand panel or under the Tools menu).

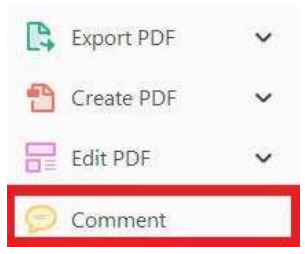

This will open up a ribbon panel at the top of the document. Using a tool will place a comment in the right-hand panel. The tools you will use for annotating your proof are shown below:

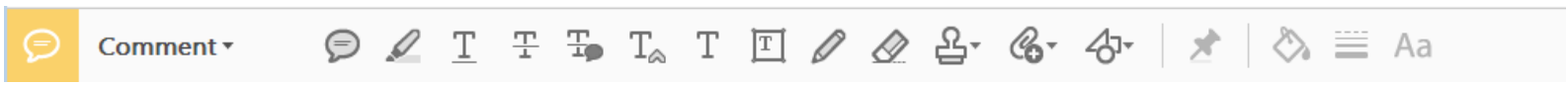

1. Replace (Ins) Tool – for replacing text.

Strikes a line through text and opens up a text box where replacement text can be entered.

How to use it:

- Highlight a word or sentence.
- Click on .
- Type the replacement text into the blue box that appears.

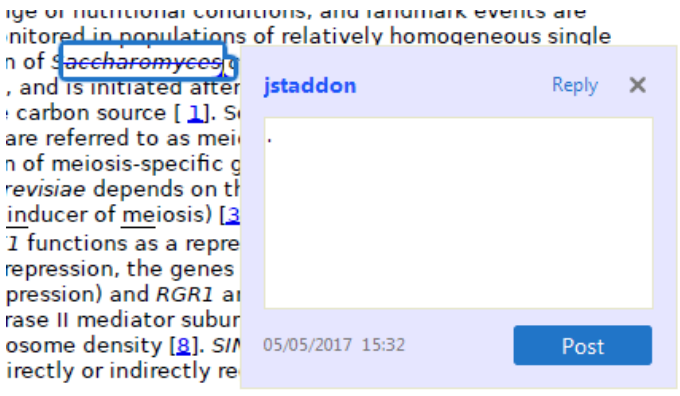

2. Strikethrough (Del) Tool – for deleting text.

Strikes a red line through text that is to be deleted.

How to use it:

- Highlight a word or sentence.
- Click on .
- The text will be struck out in red.

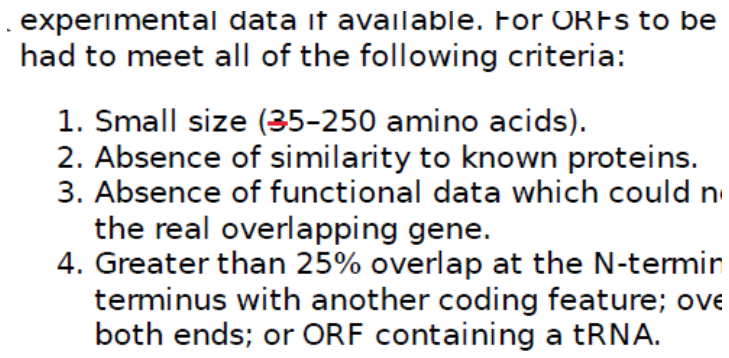

3. Commenting Tool – for highlighting a section to be changed to bold or italic or for general comments.

Use these 2 tools to highlight the text where a comment is then made.

How to use it:

- Click on .
- Click and drag over the text you need to highlight for the comment you will add.
- Click on .
- Click close to the text you just highlighted.
- Type any instructions regarding the text to be altered into the box that appears.

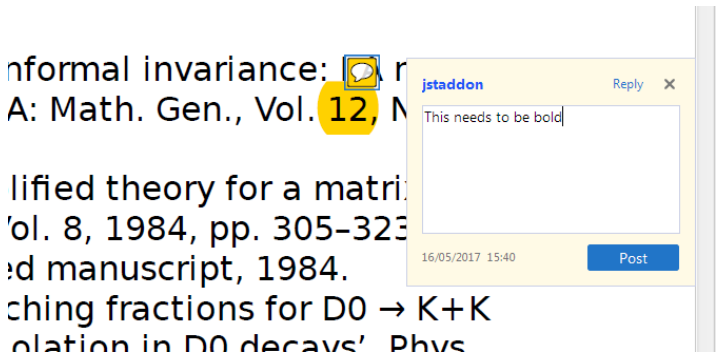

4. Insert Tool – for inserting missing text at specific points in the text.

Marks an insertion point in the text and opens up a text box where comments can be entered.

How to use it:

- Click on .
- Click at the point in the proof where the comment should be inserted.
- Type the comment into the box that appears.

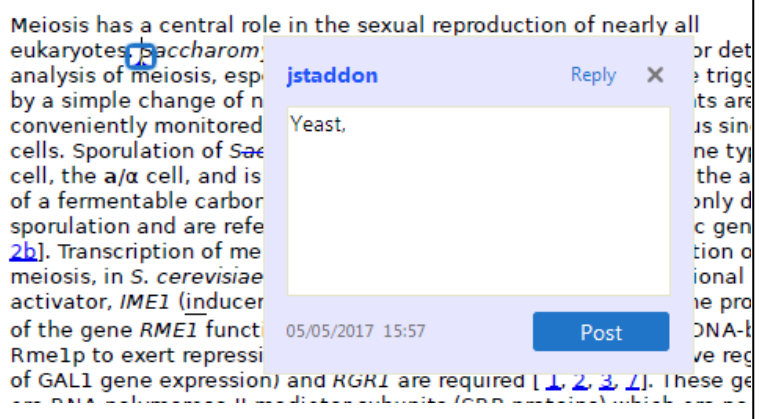

WILEY

USING e-ANNOTATION TOOLS FOR ELECTRONIC PROOF CORRECTION

5. Attach File Tool – for inserting large amounts of text or replacement figures.

Inserts an icon linking to the attached file in the appropriate place in the text.

How to use it:

- Click on  .
- Click on the proof to where you'd like the attached file to be linked.
- Select the file to be attached from your computer or network.
- Select the colour and type of icon that will appear in the proof. Click OK.

  The attachment appears in the right-hand panel.

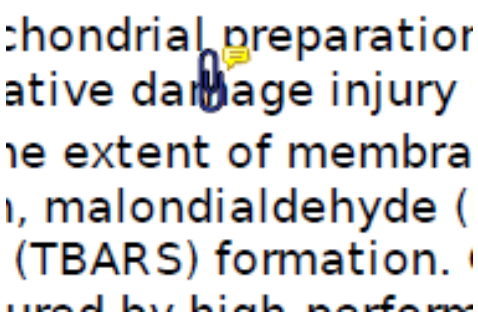

6. Add stamp Tool – for approving a proof if no corrections are required.

Inserts a selected stamp onto an appropriate place in the proof.

How to use it:

- Click on  .
- Select the stamp you want to use. (The Approved stamp is usually available directly in the menu that appears. Others are shown under *Dynamic*, *Sign Here*, *Standard Business*).
- Fill in any details and then click on the proof where you'd like the stamp to appear. (Where a proof is to be approved as it is, this would normally be on the first page).

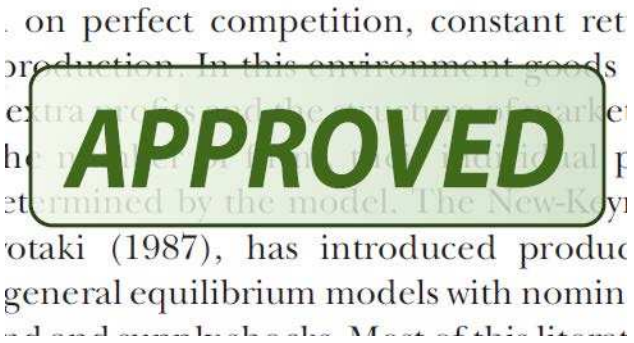

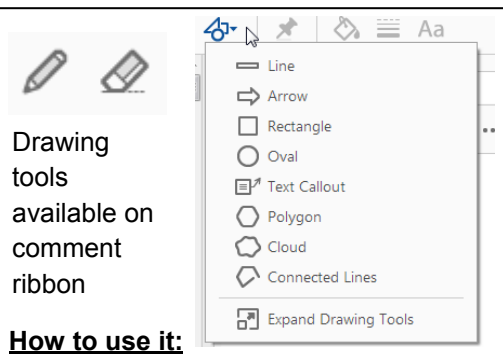

Drawing tools available on comment ribbon

7. Drawing Markups Tools – for drawing shapes, lines, and freeform annotations on proofs and commenting on these marks.

Allows shapes, lines, and freeform annotations to be drawn on proofs and for comments to be made on these marks.

How to use it:

- Click on one of the shapes in the Drawing Markups section.
- Click on the proof at the relevant point and draw the selected shape with the cursor.
- To add a comment to the drawn shape, right-click on shape and select *Open Pop-up Note.*
- Type any text in the red box that appears.

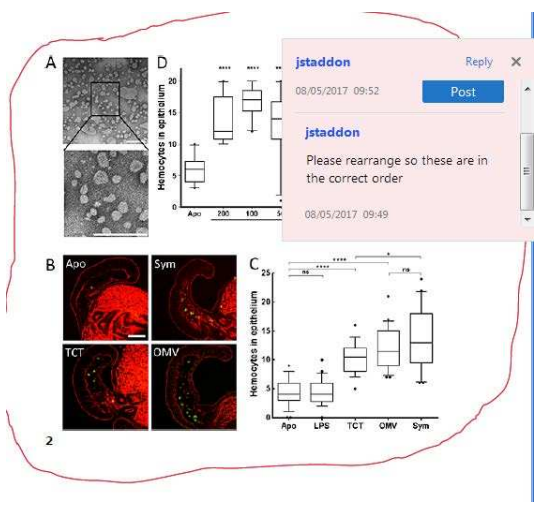

For further information on how to annotate proofs, click on the Help menu to reveal a list of further options: